# Supporting Information

# Excellent graphitic carbon nitride nanosheets-based photoelectrochemical platform motivated by Schottky barrier and LSPR effect and its sensing application

Hong Dai,[a*] Shupei Zhang,[a] Yilin Li,[a] Yanyu Lin [a,b]

a College of Chemistry and Chemical Engineering, Fujian Normal University, Fuzhou 350108, P. R. China

b Ministry of Education Key Laboratory of Analysis and Detection for Food Safety, and Department of Chemistry, Fuzhou University, Fuzhou 350002, P. R. China

## Experimental

### Apparatus

The morphologies and sizes of g-$C_3N_4$ and Au NRs were observed by Scanning electron microscopy (SEM, Hitachi S-4800) and Transmission electron microscopy (TEM, FEI F20 S-TWIN), respectively. The chemical composition of g-$C_3N_4$ was characterized by X-ray spectroscopy (XPS, VG 2000) using Al-$K_\alpha$ monochromated radiation as the exciting source. The UV-vis light absorption spectra were obtained from a Hitachi UV-3010 spectrophotometer. Cyclic voltammetry (CV), Linear Sweep Voltammetry (LSV), Amperometric i-t Curve, and Electrochemical Impedance Spectroscopy (EIS) were performed on a CHI 760 electrochemical workstation (Shanghai Chenhua Instrument Co., China) with a conventional three-electrode cell. An Ag/AgCl electrode (sat. KCl) was used as reference electrode and a platinum wire was used as counter electrode, respectively. A modified glassy carbon electrode (3 mm in diameter) was used as working electrode. All the PEC measurements were performed with a homemade PEC system in PBS (0.1 M, pH 7.0) containing 1 mM $H_2O_2$ which was deaerated with high-purity nitrogen. The pH measurements were carried out on PHS-3C exact digital pH metre (Shanghai Leici Co. Ltd., China), which was calibrated with standard pH buffer solutions.

### Synthesis of g-$C_3N_4$ nanosheets

In a typical synthesis, g-$C_3N_4$ were prepared by directly heating melamine.[S1] Firstly, 15.0 g of white melamine powder was placed into a porcelain boat and heated at 823K for 4 h in a tube furnace under open air condition. Then the production was cooled to room temperature to obtain the primrose yellow g-$C_3N_4$ product. Afterwards, 30 mg of the prepared g-$C_3N_4$ power was added into 3 mL redistilled water and the suspension was ultrasonicated for 8 h to ensure g-$C_3N_4$ can get a good dispersion, the stock solution of 10 mg $mL^{-1}$ was prepared for the further use.

### Synthesis of Au NRs

Au NRs were prepared via a commonly known seed-mediated growth approach reported elsewhere.[S2] First, 500 μL of 10 mM $HAuCl_4$ was added into 15 mL of 0.1 M CTAB solution. Successively, 1.2 mL of ice-old 10 mM $NaBH_4$ was quickly added with vigorous stirring for 2 min, and the solution was kept undisturbed at room temperature for at least 10 min before use, which obtained the seed solution. Then, 50 mL of seed solution was added to the growth solution (25 mL of 0.2 M CTAB, 2.5 mL of 0.01 M $HAuCl_4$, 0.3 mL of 10 mM $AgNO_3$, 21.1 mL distilled water, 2.75 mL of 0.01 M L-ascorbic acid) vigorously stirred for 20 s, and then allowed to initiate the growth of the Au NRs for 12 h. Finally, the stock Au NRs were collected by centrifugation at 8000 rpm for 10 min to remove the excess CTAB and then the Au NRs solution was diluted to the original volume for the future use.

Table S1 The results XPS of g-$C_3N_4$ nanosheets

| Element | Series unn. (wt.%) | C norm. (wt.%) | C Atom. (at.%) | C Error (1 Sigma) (wt.%) |
|---|---|---|---|---|
| C | K-series 44 | 44 | 3.95 | 10.08 |
| N | K-series 50.84 | 50.84 | 55.45 | 8.39 |
| O | K-series 5.16 | 5.16 | 98.34 | 2.21 |

As demonstrated in Table S1, the atomic ratio of carbon and nitrogen was 3 to 4, which proved that the g-$C_3N_4$ was successfully synthesized in this work.

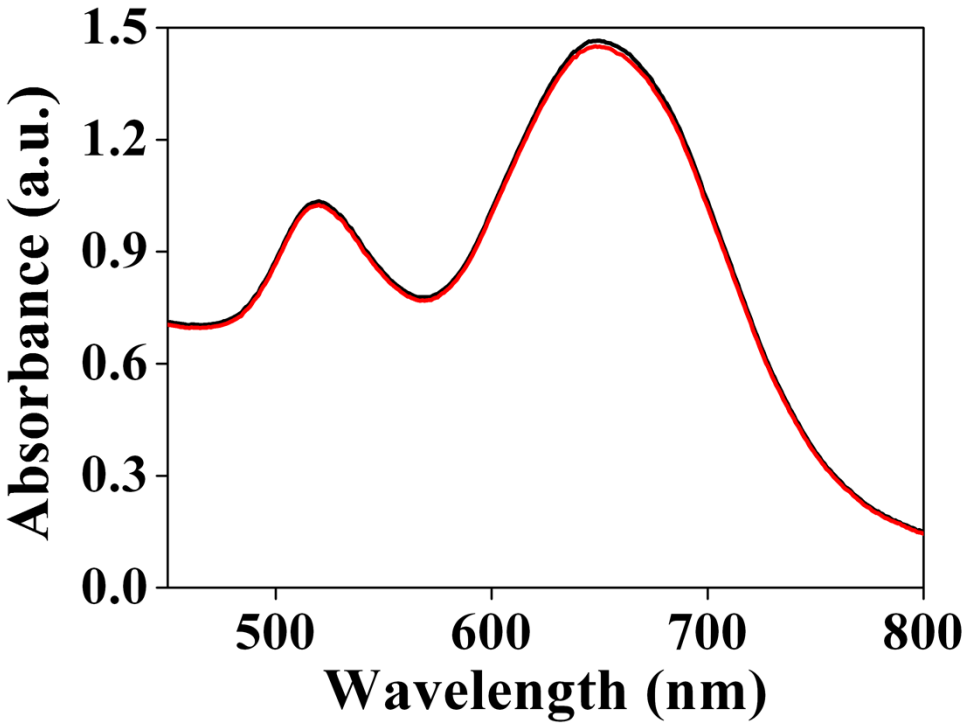


Figure S1. UV-vis absorption spectra of Au NRs at different time (black: fresh, red: stored in room temperature for 3 days).

To further prove the stability of gold nanorods, the UV-vis absorption spectra of Au NRs at different time was explored. As demonstrated in Fig. S1, the UV-Vis spectra of Au NRs all showed two absorption peaks, which the weak and strong absorption peak correspond to the excitation of LSPR mode along the transverse and longitudinal directions, respectively. As expected, the two curves are almost superposable, demonstrating that the good stability of Au NRs prepared in the work.

**Photoconversion efficiency of the hybrid**

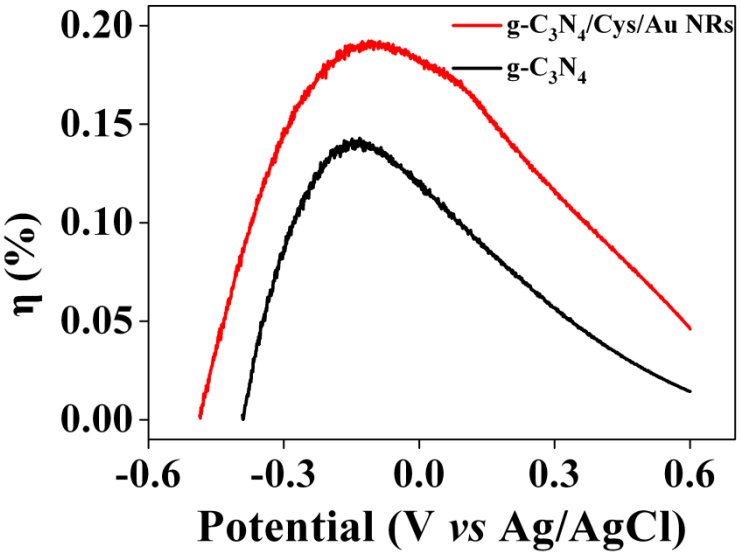


**Fig. S2** The photoconversion efficiencies of g-$C_3N_4$ (black line) and g-$C_3N_4$/Cys/Au NRs (red line).

The photoconversion efficiency (η) of photoelectrodes in the presence of an external applied potential $E_{app}$, was calculated via the equation:[S3-S4]

$$\eta(\%) = \frac{j_p \times \left(E^0_{rev} - \left|E_{meas} - E_{aoc}\right|\right)}{I_0} \times 100 \qquad (1)$$

where $j_p$ stands for the photocurrent density (mA $cm^{-2}$), $I_0$ represents the intensity of the incident light (86 mW $cm^{-2}$), $E^0_{rev}$ is the standard state-reversible potential which is 1.23 V(vs. NHE), $\left|E_{app}\right|$ is the absolute value of the applied potential $E_{app}$, $E_{meas}$ is the electrode potential (vs. Ag/AgCl) of the working electrode at which the $j_p$ is measured, and $E_{aoc}$ is the electrode potential of the same working electrode at open circuit, which is measured under the same illumination and in the same electrolyte solution at which $j_p$ is measured. As demonstrated in the inset of Fig. 2C, the photoconversion efficiency of g-$C_3N_4$ improved after the incorporation of Au NRs, exhibiting the g-$C_3N_4$/Cys/Au NRs possessed higher photocatalytic activity, which agreed well with the results of LSV experiments.

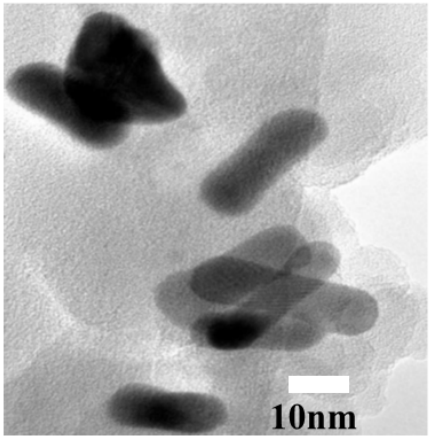


**Fig. S3** TEM images of g-$C_3N_4$/Cys/Au NRs hybrid.

To further demonstrate the assembly, as shown in TEM image, after introduction of Au NRs on functional g-$C_3N_4$ layer, the Au nanorods were deposited upon the surface of g-$C_3N_4$ sheets. The Au NRs could be found on the planer of g-$C_3N_4$ constituting an intact bonding with g-$C_3N_4$ through Au-S bond provided by poly(L-cysteine), which revealed the successful self-assembly of Au nanorods.

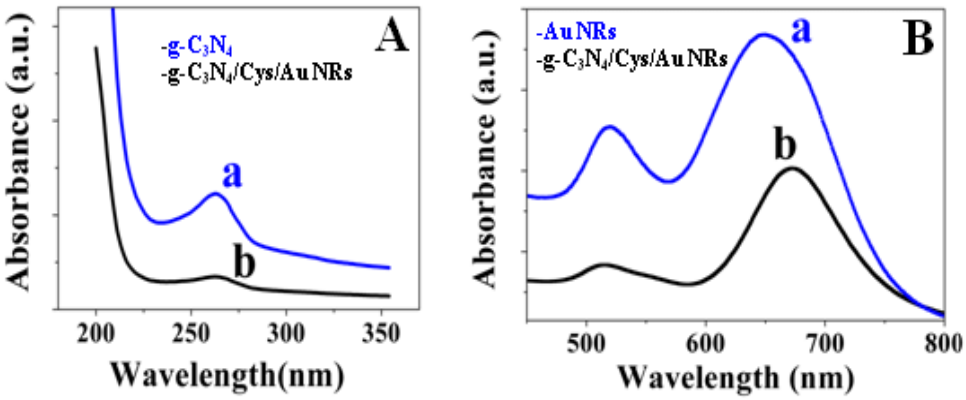


**Fig. S4** UV-vis absorption spectrum of g-$C_3N_4$, Au NRs and g-$C_3N_4$/Cys/Au NRs hybrid.

The photoabsorption behaviors of the prepared g-$C_3N_4$ and g-$C_3N_4$/Cys/Au NRs composites were investigated by using UV-vis absorption spectroscopy. As exhibited in Fig. S4A, the pure g-$C_3N_4$ has strong absorption at 261 nm. Noticeably, after the self-assemble of Au NRs to the g-$C_3N_4$ via L-cysteine, the characteristic absorbance peak of g-$C_3N_4$ (curve b in Fig. S4A) still existed but the absorption edges of the composites shifted to the longer wavelength region of 268 nm and became smooth in comparison with that of pure g-$C_3N_4$ (curve a in Fig. S4A) which was in consistent with the previous research work[S5-S6], demonstrating the successful self-assembly of Au NRs. Additionally, the curve a in Fig. S4B displayed the two characteristic absorption peaks of 525 nm and 649 nm of the sheer Au NRs, however, after the Au NRs were self-assembled, the peak of 525 nm was hardly shifted because of it belongs to the Au nanoparticles which were not deposited on the g-$C_3N_4$ nanosheets. Nevertheless, the peak of 649 nm was moved to 672 nm which obviously occurred to red shift and enhanced the incident light absorption ability, leading to excite more electrons and holes and further enhance the photocurrent of g-$C_3N_4$.[S7] The absorption edge of the composite shifted to longer wavelength is also in agreement with the former investigation[S8], revealing the successful self-assembly of Au NRs to g-$C_3N_4$ functionalized by Cys.

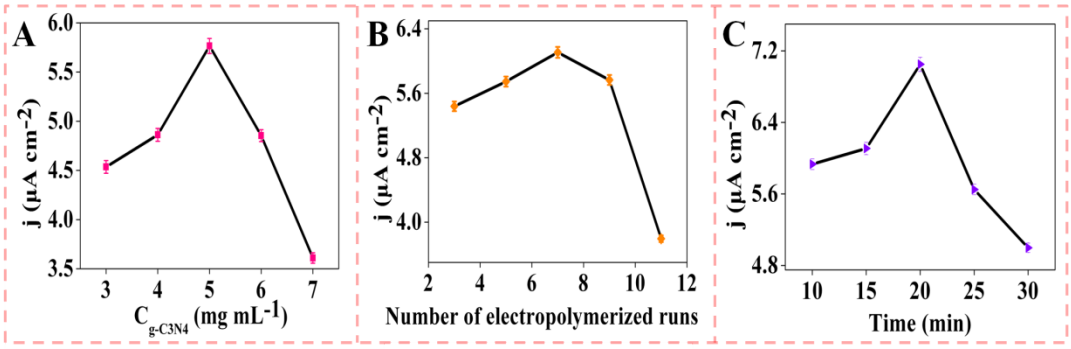


**Fig. S5** Effect of (A) the concentration of g-$C_3N_4$, (B) electropolymerized runs, (C) Au NRs self-assembly time to the photocurrent density of GCE/g-$C_3N_4$/Cys/Au NRs in 0.1 M PBS containing 1 mM of $H_2O_2$.

**Control of conditions in fabricating of PEC hybrid**

To investigate the effect of g-$C_3N_4$ film thickness which is an important influencing factor for the sensitivity of the PEC biosensor, the photocurrent responses of different concentrations of g-$C_3N_4$ were demonstrated in Fig. S5A. As was shown, the photocurrent significant increased until 5 mg $mL^{-1}$ g-$C_3N_4$ was dropped on the electrode surface and then decreased rapidly. It could be explained as the fact that the more the immobilized amount of g-$C_3N_4$, the more photogenerated electrons from the outer g-$C_3N_4$ to electrode surface to improve the photocurrent. However, the thicker g-$C_3N_4$ film impeded the electrons be captured by electrode, leading to the photocurrent decreased with further increasing.

Fig. S5B exhibited the photocurrent density gradually increased with the increasing of electro-polymeric numbers from 3 to 7, ascribing to the increasing of Cys amount which contacted more Au NRs to the electrode. Subsequently, the photocurrent descend drastically because that the excessive Cys resulted in thicker film, leading to the increasing of internal resistance, causing the photocurrent descended. Therefore, 7 cycles was selected throughout the subsequent measurements.

To optimize the amount of Au NRs, different self-assemble time of Au NRs were explored to fabricate the GCE/g-$C_3N_4$/Cys/Au NRs electrode. As illustrated in Fig. S5C, with the self-assembled time increasing, the

more visible light was absorbed and more photogenerated electrons were driven to electrode surface due to that more Au NRs enhanced the LSPR effect in the hybrid. As a result, the reason above can be taken into account for significant increasing of photocurrent response. Nevertheless, a deterioration of the photocurrent density was obtained with a further enhancement of the self-assembled time, attributing to the thicker Au film would gathered together and impeded the transfer of the electrons from the outside layer of Au NRs to the electrode, leading to the photocurrent responses descended. For the sake of a significant photocurrent signal and higher sensitivity, 20 min was chosen as the optimized time for the signal recording in the following experiments.

**Characterizing the fabrication process of the sensor**

Fig. 3B depicted the stepwise photocurrent changes during the assembly of functionalized electrodes. Comparing with curve a, there was a strong photocurrent was observed on GCE/g-$C_3N_4$ (curve b), which revealed the good PEC performance of the g-$C_3N_4$. Then the photocurrent decreased after the electrochemical polymerization of GCE/g-$C_3N_4$ (curve c) due to that the forming of Cys layer which impeded the transfer of electrons and absorption of incident light. Subsequently, when Au NRs were assembled successfully on the surfaces of GCE/g-$C_3N_4$/Cys, as expected, the photocurrent (curve d) significantly elevated due to the Schottky barrier and LSPR effect in the hybrid. And after the modified electrode was assembled with CD, the photocurrent response (curve e) reduced attributing to the CD as an inert layer which impeded the transfer of electrons. Similarly, the photocurrent dramatically decreased after the modified electrode was soaked into 10 μM of NA solution for 20 min, which was ascribed to that the absorption of NA onto the modified electrode blocked the access of the redox to the electrode, indicating that the NA can be successful specific recognized by GCE/g-$C_3N_4$/Cys/Au NRs/CD. These findings future verified the successful fabrication of modified electrode and the truth of the proposed hypothesis.

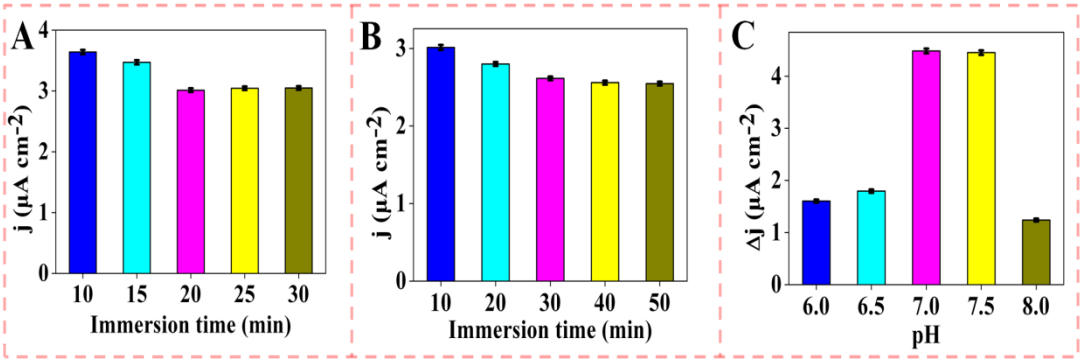


**Fig. S6** Effect of (A) CD self-assembled time , (B) Hat self-assembled time and (C) solution pH to the photocurrent density at the GCE/g-$C_3N_4$/Cys/Au NRs/CD/Het/NA in 0.1 M PBS containing 1 mM of $H_2O_2$.

**Optimization of detection condition**

The self-assembled time of CD onto GCE/g-$C_3N_4$/Cys/Au NRs is an important factor relevant to the PEC detection. As shown in Fig. S6A, the photocurrent response on the PEC biosensor declined upon the increasing immersion time in 1 mg $mL^{-1}$ CD from 10 min to 20 min, then the photocurrent remained stable. Therefore, considering the optimal analytical performance, the self-assembled time of 20 min was selected in the future study. Besides, the recognize time between NA and CD also influence the sensitivity of sensor. As demonstrated in Fig. S6B, the photocurrent density reached nearly a plateau after 30 min in the presence of 10 μM NA, indicating that abundant NA permeated into the cavity of CD at the time of 30 min. So, 30 min was used as the optimal recognize time. According to the results exhibited in Fig. S6C, it could be concluded that the maximum Δj (j = j – $j_0$, j and $j_0$ are the photocurrent density of the GCE/g-$C_3N_4$/Cys/Au NRs/CD electrode prior to and after interacted NA) was obtained at pH 7.0. In order to ensure the large Δj, pH 7.0 PBS was selected in following measurements.

**Optimization of blocking agents**

To avoid or minimize non-specific adsorptions of NA on GCE/g-$C_3N_4$/Cys/Au NRs/CD surface, various studies about blocking agents on the electrode surface were investigated in Fig. 3D. As demonstrated in curve a, a classic pair of redox peaks was obtained at GCE/g-$C_3N_4$/Cys/Au NRs/CD, implying there still existed remaining unmodified Au sites. Therefore, it is necessary to select blocking agents to block the remaining Au sites. Cleary, the currents and the peaks at modified electrodes which were blocked by different blocking agents were declined gradually from curve b to curve c. The phenomenon can be explained by that the benzene ring of p-mercaptobenzoic acid and p-aminothiophenol hindered the more blocking agents assembled onto the surface, leading to more remaining Au sites. Whereas, the presence of Hat film significantly reduced the redox peaks on the electrode, owing to Hat almost completely blocked the remaining Au sites on the modified electrode. Therefore, in the following experimentations, we chose the Hat as the blocking agent.

**Stability**

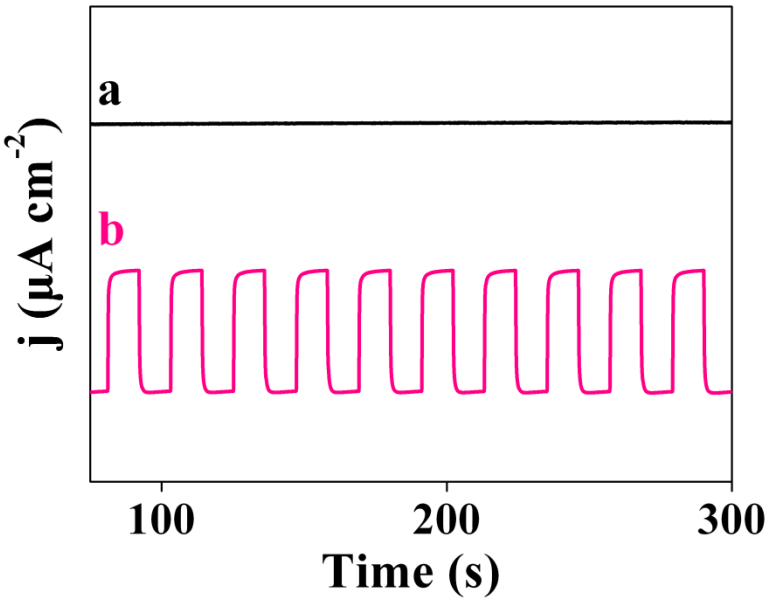


**Fig. S7** The photocurrent density of the GCE/g-$C_3N_4$/Cys/Au NRs/CD/Het was self-assembled with 10 μM of NA (a) under continues and (b) repeated on and off cycles simulated visible light in 0.1 M PBS solution containing 1 mM $H_2O_2$.

Table S2 Figures of merits of comparable methods for determination of NA

| Method | Linear ranges (μmol/L) | Detection limit (μmol/L) | Reference |
|---|---|---|---|
| CE-DAD | 2.5-100 | 0.143 | S9 |
| UPLC-DAD-QTOF | 0.276-8.61 | 0.05 | S10 |
| ECL | 0.001-1 | 0.0008 | S11 |
| PEC | 0.0001-100 | 0.00003 | This work |

UPLC-DAD-QTOF ultra high performance liquid chromatography-diode array detector-quadrupole time-of-flight tandem mass spectrometry; CE-DAD capillary electrophoresis-diode array detector; ECL electrochemiluminescene

Table S3 The results of addition recovery test (n=3)

| Content in samples (μmol $L^{-1}$) | Addition (μmol $L^{-1}$) | Measured (μmol $L^{-1}$) | Recovery (%) |
|---|---|---|---|
| 20.1 | 0.001 | 18.923 | 94.14 |
| 20.1 | 0.1 | 21.0 | 103.96 |
| 20.1 | 10 | 29.6 | 98.34 |

n is the repetitive measurements number

**Reference**


S1 C. M. Cheng, Y. Huang, X. Q. Tian, B. Z. Zheng, Y. Li, H. Y. Yuan, D. Xiao, S. P. Xie and M. M. Choi, *Anal. Chem.*, 2012, **84**, 4754.

S2 L. H. Guo, Y. J. Huang, Y. Kikutani, Y. Tanaka, T. Kitamori and D. -H. Kim, *Lab Chip*, 2011, **11**, 3299.

S3 S. U. M. Khan, M. Al-Shahry and W. B. Ingler, *Science*, 2002, **297**, 2243.

S4 Y. Hou, X. Y Li, Q. D. Zhao, X. Quan, G. H. Chen, *Adv. Funct. Mater.*, 2010, **20**, 2165.

S5 S. Q. Chang, A. Y. Xie, S. Chen and J. Xiang, *J. Electroanal. Chem.*, 2014, **719**, 86.

S6 S. Samanta, S. Martha and K. Parida, *ChemCatChem*, 2014, **6**, 1453.

S7 L. C. Chen, X. T. Zeng, P. Si, Y. M. Chen, Y. W. Chi, D. H. Kim and G. N. Chen, *Anal. Chem.*,2014, **86**, 4188.

S8 T. Q. Han, X. J. Li, Y. Y. Li, W. Cao, D. Wu, B. Du and Q. Wei, *Sens. Actuators, B.* 2014, **205**, 174.

S9 S. Sanl and C. Lunte, *Anal. Methods*, 2014, **6**, 3858.

S10 J. Dong, Y. Zhu, X. M. Gao, Y. X. Chang, M. Wang and P. Zhang, *J. Pharm. Biomed. Anal.*, 2013, **80**, 50.

S11 H. Dai, C. P. Yang, X. L. Ma, Y. Y. Lin and G. N. Chen, *Chem. Commun.*, 2011, **47**, 11915.